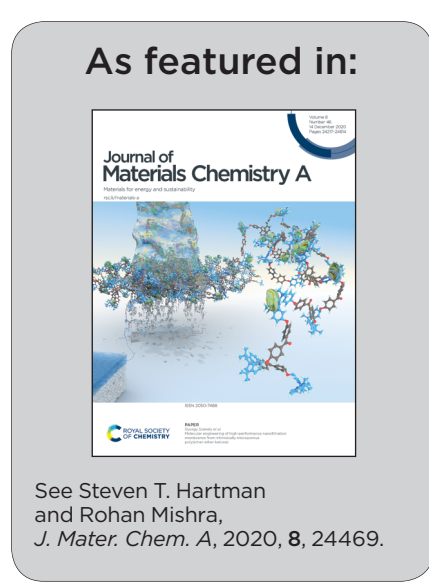


Highlighting a study on layered electrides as intercalation anodes for fluorine ion batteries by Dr. Steven Hartman and Prof. Rohan Mishra from Washington University in St. Louis.

Layered electrides as fluoride intercalation anodes

The fluoride ion is well suited to be the active species of rechargeable batteries, due to its small size, light weight, and high electronegativity. Here, layered electrides, such as Ca_2N and Y_2C — that have an electron occupying a lattice site — are predicted as promising hosts for fluoride intercalation, since their anionic electrons create large interstices, and their open layered structure enables fast diffusivity.





Journal of Materials Chemistry A



PAPER

View Article Online



Cite this: J. Mater. Chem. A, 2020, 8,

Steven T. Hartman (1) ‡ and Rohan Mishra (1) *ab

The fluoride ion is well suited to be the active species of rechargeable batteries, due to its small size, light weight, and high electronegativity. While existing F-ion batteries based on conversion chemistry suffer from rapid electrode degradation with cycling, those based on fluoride intercalation are currently less attractive then cation intercalation battery chemistries due to their low reversible energy densities. Here, using firstprinciples density-functional-theory calculations, we predict that layered electrides, such as Ca₂N and Y₂C - that have an electron occupying a lattice site - are promising hosts for fluoride intercalation, since their anionic electrons create large interstices. Our calculations indicate that anodes made from layered electrides can offer voltage up to -2.86 V vs. La_2CoO_4 cathode, capacity >250 mA h g⁻¹, and fast diffusion kinetics with migration barriers as low as 0.15 eV. These metrics compare favorably to popular Li-ion intercalation cathodes such as LiCoO2. Electrides open up a new space for designing fluorine intercalation batteries with good performance and cyclability.

Layered electrides as fluoride intercalation anodes†

Received 22nd June 2020 Accepted 29th September 2020

DOI: 10.1039/d0ta06162j

rsc.li/materials-a

Rechargeable batteries enable crucial modern technologies, such as mobile phones, electric cars, and aerial drones, and will be required in even larger numbers for the rapidly growing automotive fleets and grid-scale storage of electricity generated by intermittent renewable sources. Currently, the market is dominated by Li-ion batteries, which shuttle lithium ions between two intercalation electrodes such as graphite and LiCoO₂. In these electrodes, the Li ions move into empty spaces in a host material without significantly disrupting the host's structure. While this design has achieved high energy density and adequate cycling stability, the supply risk of lithium and cobalt¹ is predicted to create obstacles for the surge in battery usage. Current Li-ion batteries also pose safety concerns due to Li dendrite growth and thermal runaway.2 Therefore, it is desirable to find other high-performance battery chemistries besides Li-ion.

The search for alternative chemistries has primarily been limited to light cations such as Na⁺, ³ K⁺, ⁴ Mg²⁺, ⁵ Zn²⁺, ⁶ and Al³⁺. ⁷ A handful of studies have instead focused on using anions as the active species.^{8,9} Amongst the various candidates for active anion batteries, fluoride (F-) is especially attractive due to its earth-abundance, light weight, high electronegativity, and reasonably fast diffusion in liquid or solid electrolytes. 10-17 In

contrast to the success of Li batteries using two intercalation electrodes, most research on fluoride-ion batteries (FiBs) has followed a different path involving conversion reactions, 18,19 pairing metals with metal fluorides, such as:11 3Sn + 2BiF₃ → $3SnF_2 + 2Bi$.

The theoretical current capacity of conversion electrodes can be very high, such as 669 mA h g⁻¹ for Ca/CaF₂, compared to 294 mA h g⁻¹ for LiCoO₂. However, these high capacities are difficult to achieve in practice. The phase transformation of the metal to its fluoride during charge/discharge cycles is typically a slow reaction which requires a large overpotential; furthermore, if the resulting volume change is large, the electrode can crumble and degrade during repeated cycling.20 In addition, the pure metal electrode sometimes dissolves into the electrolyte, further degrading it.19 These effects are also seen in Li-ion conversion batteries, which have not found commercial success despite extensive research.21 Therefore, prior experience suggests the value of intercalation FiBs, but high-capacity, fluoride intercalation electrodes have been not been reported. The first F⁻ intercalation electrode to be tested was LaSrMnO₄/ LaSrMnO₄F₂, which offered a moderate theoretical capacity of 172 mA h g⁻¹, but proved to have very limited reversibility due to destructive side reactions and overpotentials >1 V. La₂CoO₄/ La2CoO4F later provided improved cycling durability, but at the cost of low theoretical capacity (67 mA h g⁻¹). These electrodes have relatively little driving force for fluoride intercalation, making them suitable for cathodes, while FiB intercalation anodes have not yet been demonstrated.

In this article, we take a new approach to design intercalation FiBs, which is to use the unconventional chemistry of electride crystals to our advantage. These inorganic electrides have interstices occupied by electrons that act as anions, due to

aInstitute of Materials Science and Engineering, Washington University in St. Louis, One Brookings Drive, St. Louis, MO 63130, USA. E-mail: steven.t.hartman@wustl.edu ^bDepartment of Mechanical Engineering and Materials Science, Washington University in St. Louis, One Brookings Drive, St. Louis, MO 63130, USA. E-mail: rmishra@wustl. edu

[†] Electronic supplementary information (ESI) available: Performance metrics of other anode materials investigated in this study; effect of van der Waals corrections; decomposition pathways; AIMD data. See DOI: 10.1039/d0ta06162j

[‡] Present Address: Materials Science and Technology Division, Los Alamos National Laboratory, Los Alamos, NM 87545, USA,

their unusual stoichiometries, which are not charge-balanced in common oxidation states.²³ We use first-principles densityfunctional-theory (DFT) calculations to show that electrides can intercalate fluoride stably by replacing the anionic electron with a F⁻. Among the 12 known or predicted electrides which we have examined, we predict Ca₂N and Y₂C as promising candidates for intercalation anodes with theoretical gravimetric capacities \sim 280 mA h g⁻¹, volume change during cycling <15%, voltage <-2.5 V νs. La₂CoO₄ cathode, and low kinetic barriers <0.2 eV for fluoride ion transport. These values approach the performance of popular Li-ion electrodes such as LiCoO₂, which has a theoretical capacity 295 mA h g⁻¹, calculated voltage 3.7 V vs. graphite, and migration barriers ~0.3 eV,24 and Ca2N in particular is much more earth-abundant than LiCoO2. The excellent performance metrics of Ca2N and Y2C, if realized experimentally, will be a major step toward the practical use of FiBs.

First, we consider the crystal structures of Li-intercalation electrodes, to see if the proven design principles can be transferred directly to FiBs. Two of the most successful Li⁺ intercalation cathodes, LiFePO₄ (ref. 25) and LiCoO₂,²⁶ are shown in Fig. 1a and b, respectively. They are characterized by anionic polyhedra that are centered on small, highly charged cations (Shannon radius of 0.65 Å for Fe³⁺, 0.17 Å for P⁵⁺, and 0.53 Å for Co⁴⁺). The Li⁺ ions rest in the interstices between these polyhedra. The transition metal ions, besides providing the redox activity by changing their oxidation state, also serve to hold the crystal together when the Li⁺ is absent (in the charged state). Thanks to these framework-preserving cations, LiCoO₂ and

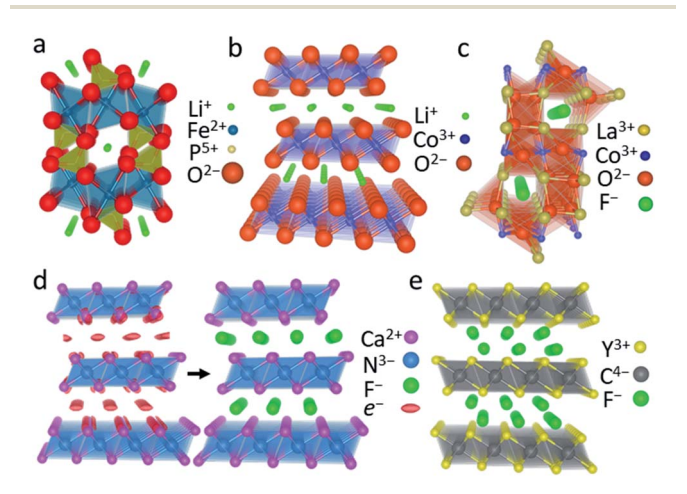


Fig. 1 Structural principles for fluorine intercalation electrode design. (a) The popular Li-ion intercalation electrode LiFePO₄, in which Li⁺ (green) occupies distorted octahedral sites between PO₄ tetrahedra and FeO₆ distorted octahedra. (b) LiCoO₂, with Li⁺ sitting in octahedral interstices between layers of edge-sharing CoO₆ octahedra. (c) The previously known F⁻ intercalation electrode La₂CoO₄F, with F⁻ (green) in tetrahedral interstices between strongly distorted La₅CoO octahedra. (d) The newly proposed Ca₂NF electrode, with F⁻ in octahedral interstices between layers of edge-sharing Ca₆N octahedra. The localized anionic electrons (red) between the Ca₂N layers are shown with isosurfaces of the electron localization function. Ca₂NF's structure is the inverse of LiCoO₂'s structure in (b). (e) Y₂CF₂, with F⁻ in tetrahedral interstices between layers of edge-sharing Y₆C octahedra.

LiFePO₄ have calculated volume changes of only 3% and 7%,²⁴ respectively, as Li is removed, promoting durability over many cycles.

Based on these examples, to intercalate F-, we ought to invert the paradigm and have cationic polyhedra centered on some other anion, to maintain the structural integrity in the absence of F⁻ ions. However, we immediately notice that anions are generally larger than cations, 27 with F having the smallest Shannon radius of 1.33 Å. In addition to making fluoride intercalation more challenging, the large size of anions also restricts the construction of anion-centered polyhedra. Therefore, the best candidates for anion-centered polyhedra are the first-row species $N^{3-}(1.46 \text{ Å})$, B^{3-} , C^{4-} , and possibly $O^{2-}(1.4 \text{ A})$ Å).28,29 As for the surrounding cations, they should be large enough to create stable polyhedra with spacious interstices between them. They should also have a low charge to achieve charge balance, since they are more numerous than the central anion even if the polyhedra share many edges and faces. The cation also needs to be light for good gravimetric capacity, and inexpensive. Finally, it ought to be redox-active, with several stable oxidation states.

These constraints are not easily satisfied by a single cation, and indeed all existing fluoride intercalation electrodes combine two or more cation species. Fig. 1c shows the most successful electrode to date, La₂CoO₄F, 18,22 which uses the larger La³⁺ cations (1.16 Å) to create large tetrahedral sites for F $^-$ in the rock-salt structured LaO layers. The smaller Co²⁺ (0.65 Å) occupies CoO₂ layers which provide the redox activity, as F $^-$ intercalation onto the LaO layers oxidizes Co to 3+. However, the gravimetric capacity is low (67 mA h g $^{-1}$ theoretically) because the heavy La is "dead weight" from an electrochemical perspective. This is generally true for similar electrodes such as MgFeSb₄O₈F (39 mA h $^{-1}$ g)³⁰ or FeSb₂O₄F (74 mA h g $^{-1}$) although it can be mitigated by using cations lighter than La or Sb, such as Sr (1.26 Å) in Sr₂TiO₃F₂ (197 mA h g $^{-1}$), which has been proposed as a FiB anode but not yet tested.

We conclude that to keep the electrode light, yet retain large interstitial sites, it should ideally have only one type of cation. Alkali and alkaline earth metals are light, large, inexpensive, and have low charge, satisfying all the constraints except redox activity, so we can expect good results if these metals can be stabilized in oxidation states besides +1 and +2, respectively. Such materials are rare, but a small group of suboxides, subnitrides, and hypocarbides are stable with fewer anions than would be expected by charge balance.33 One well-studied example is the electride Ca2N, which from a chemical perspective can be represented as Ca₂²⁺N³⁻e⁻, where e⁻ is an electron localized at an empty anion site. We show the structure of Ca2N in Fig. 1d. Ca2N has an inverse LiCoO2 structure, with Ca₆N octahedra instead of CoO₆, and Li replaced by anionic electrons. This suggests the following half-reaction can proceed topochemically, with little volume change:

$$Ca_2N + F^- \rightarrow Ca_2NF + e^-$$
 (1)

While Ca₂N is referenced as a possible FiB electrode in a patent application,³⁴ any related studies remain unpublished

beyond a single voltammogram, so a detailed theoretical study offers the first opportunity to understand the F⁻ intercalation properties of Ca2N.

To assess the intercalation of Ca₂N with F⁻ ions, we have calculated the stability of the products and reactants for a variety of fluoride intercalation reactions along with the associated change in voltage and volume using DFT. For details of these calculations, see the section on Computational methods. We find that both Ca2N and Ca2NF, with their structures shown in Fig. 1d, are on the convex hull, and hence, stable against decomposition into known competing phases present in the Materials Project database.24 The fluoride ion occupies the octahedral site between Ca2N layers, while the tetrahedral sites, which are twice as many as the octahedral sites, are unoccupied. Placing fluoride into the tetrahedral site costs 0.34 eV more than the octahedral site. Upon geometry optimization, we find that Ca_2NF retains the same rhombohedral $R\bar{3}m$ phase as Ca₂N. For this structure, we can calculate its gravimetric capacity to be 285 mA h per gram of Ca2N according to

$$\frac{1 \text{ mol Ca}_2 \text{ N}}{94 \text{ g Ca}_2 \text{N}} \times \frac{1 \text{ mol e}^-}{1 \text{ mol Ca}_2 \text{N}} \times \frac{96485 \text{ A} \times \text{s}}{1 \text{ mol e}^-} \times \frac{1000 \text{ mA}}{1 \text{ A}} \times \frac{1 \text{ h}}{3600 \text{ s}} = \frac{285 \text{ mA h}}{1 \text{ g}}$$
(2)

We note that while Ca2NCl and Ca2NBr are experimentally reported to exist in the $R\bar{3}m$ phase, 35,36 Ca₂NF has only been made in the I4₁/amd phase,³⁷ which we find is 5 meV per atom higher in energy than the $R\bar{3}m$ phase. Therefore, we expect that low-temperature fluoridation, which has emerged as a successful strategy to produce fluoride structures topochemically, 38,39 should yield $R\bar{3}m$ Ca₂NF from $R\bar{3}m$ Ca₂N. Space groups $I4_1/amd$ and $R\bar{3}m$ do not have a group-subgroup relationship, so any transformation from one to the other would be a reconstructive transition,40 requiring many chemical bonds to break and reform. Once Ca2NF is kinetically trapped in the layered structure, the strength of the metal-nitride bonds will hinder the formation of other competing phases during cycling. We note that the isostructural LiCoO2/CoO2 electrode is metastable with respect to non-layered phases at both ends of the phase diagram,24 using the same computational methods we use here. CoO₂'s layered phase is metastable by 6 meV per atom relative to an I4/m phase, while LiCoO₂ has an $Fd\bar{3}m$ phase which is 193 meV per atom more stable, but careful management of the cycling can preserve the useful layered phase. The $R\bar{3}m$ phase of Ca₂NF shrinks 13% by volume during fluoridation, and the electromotive force is -2.86 V vs. La₂CoO₄/La₂CoO₄F, calculated with:

$$\frac{E_{\text{Ca}_2\text{NF}} + E_{\text{La}_2\text{CoO}_4} - E_{\text{Ca}_2\text{N}} - E_{\text{La}_2\text{CoO}_4\text{F}}}{1} = -2.86 \text{ V},$$
 (3)

where $E_{\text{Ca,NF}}$ and $E_{\text{La,CoO}_4}$ are the calculated energies of the products, $E_{\text{Ca,N}}$ and $E_{\text{La,CoO}_4\text{F}}$ are the energies of the reactants, and 1 is the number of electrons transferred in the reaction. -2.86 V is the same calculated potential as the Li/LiF halfreaction, indicating that Ca2N is highly electropositive,

consistent with its experimentally known sensitivity to air and moisture.41 Charge-balanced Ca2NF can be further fluoridated to Ca_2NF_2 at -0.78 V vs. La_2CoO_4/La_2CoO_4F , which corresponds to an oxidation of nitride to the unstable N²⁻. We do not include this in Ca₂N's theoretical capacity, since it is not clear if the anion-redox capacity is accessible without degrading the electrode. The Ca2NF2 phase is 237 meV per atom above the Materials Project convex hull, excluding species such as CaN6 which are poorly described by DFT,42 and it might decompose by nitrogen gas evolution to produce Ca₂NF and CaF₂. Therefore, it is likely necessary to cut off the reaction after the first fluoridation, such as by using a small excess of anode material.

Another electride isostructural to Ca2N, Y2C,43 is also a promising candidate for FiB anodes. Y₂C, as shown in Fig. 1e, can be represented as Y₂³⁺N³⁻2e⁻ with 2e⁻ nominally residing at the octahedral sites. Recently, Druffel et al. reported the formation of Y₂CF₂ using a high-temperature solid-state reaction of Y, YF₃, and graphite. 44 F ions are observed to occupy the tetrahedral sites between the Y₂C layers of Y₂CF₂, and the Y₂C layers re-stack from their original ABC stacking pattern to an AAA stacking in Y_2CF_2 with space group $P\bar{3}m1$, as shown in Fig. 1e. The AAA stacking of Y2C is only 28 meV per atom less stable than ABC, so it may appear as a metastable phase during charge/discharge cycles. The structural restacking may also create a significant interfacial strain between the fluoridated and unfluoridated phases, which is an important matter for further investigation. We find that Y2CF2 expands by 9% in volume relative to Y₂C, in good agreement with the 8% volume difference found experimentally. We also calculate the fluoridation voltage to be -2.56 V vs. La₂CoO₄/La₂CoO₄F, and a gravimetric capacity of 282 mA h g⁻¹.

The intermediate Y₂CF phase, with F⁻ in octahedral sites, is unstable by 81 meV per atom with respect to Y_2C and Y_2CF_2 , indicating that Y2C is likely to fluoridate in a one-step process without staging. Further evidence for a one-step reaction is provided by the formation energy of the neutral F vacancy, which we calculate to be 0.14 eV at the chemical potential defined by the Y2C/Y2CF2 equilibrium. Creating two adjacent fluoride vacancies costs 0.46 eV. Neglecting entropy, it is easier to defluoridate Y₂CF₂ all at once, than to remove one or two F at a time. Most Li-ion batteries discharge in stages because the electrostatic repulsion between Li+ gradually reduces the driving force to insert additional Li⁺, 45 but the empty octahedral F sites of the electrides can still be occupied by a negatively charged electron, so an electrostatic repulsion still occurs in the empty state. We have calculated the electrostatic interactions using VESTA,46 assuming that all anionic electrons are localized in the octahedral interstitial site. Y₂CF₂ has a total Madelung energy of -174 eV per f. u., compared to -185 eV per f. u. for Y₂C. This includes the contribution of the re-stacking; Ca₂NF does not re-stack, and has a Madelung energy of -89.5 eV per f. u., much closer to the -87.8 eV per f. u. of Ca₂N. As a comparison, the Madelung energy of $LiCoO_2$ is -110 eV per f. u. and that of CoO_2 is -140 eV per f. u.

Based on these thermodynamic calculations, we expect the layered electrides to have good energy storage capacity, but the diffusion kinetics are also important. To achieve high power

density, a battery electrode must conduct the active ion rapidly. Since the layered structures of Ca₂NF and Y₂CF₂ match LiCoO₂ so closely, it is reasonable to expect them to have fast twodimensional ion transport kinetics, which we calculate using the climbing-image nudged elastic-band (NEB) technique. 47 To provide a benchmark, we first calculate the vacancy diffusion mechanism of the known cathode material La₂CoO₄F, which is shown in Fig. 2a, with a barrier to fluoride migration of 0.83 eV. For the layered electrides, we consider three mechanisms: vacancy-assisted diffusion, direct interstitial diffusion, and interstitialcy (kick-out) diffusion. The lowest barrier for Ca2NF is the interstitialcy diffusion mechanism, in which a tetrahedral interstitial F⁻ displaces an octahedrally coordinated F⁻, forcing it into an adjacent tetrahedral interstitial site. The high-energy transition state, with a saddle point barrier height of only 0.2 eV, is associated with a configuration where the two diffusing F ions pass through triangular openings in the Ca2+ sublattice. Y₂CF₂ is more likely to exhibit vacancy diffusion, with a barrier of 0.16 eV as the F⁻ passes directly between the two Y³⁺ that are shared between the starting and ending tetrahedral sites. Both of these barriers compare favorably to the calculated barrier of 0.2-0.3 eV for Li⁺ diffusion in LiCoO₂.48

The NEB barriers assume the existence of an empty defect site (interstitial for Ca_2NF and F^- vacancy for Y_2CF_2), but the total activation energy E_A for diffusion is the formation energy of the relevant electrically neutral defect, plus the kinetic barrier height. When calculating the formation energy of the defects, we can assume either fluorine-rich and fluorine-poor conditions, which are the fluoride chemical potentials required to defluoridate or further fluoridate the electride. In Ca_2NF , the dominant mechanism switches from interstitialcy to vacancy diffusion when the fluoride chemical potential is reduced, because the fluoride interstitial costs 2.3 eV to form under fluoride-poor conditions while the F^- vacancy only costs 0.3 eV. The vacancy diffusion has a barrier of 1.34 eV which occurs as the moving F^- passes through the tetrahedral site. In contrast, we predict that Y_2CF_2 favors vacancy diffusion under any stable

fluoride potential, since the F^- vacancy's formation energy never exceeds 0.6 eV. The total calculated activation energies are 1.61–1.64 eV for Ca_2NF and 0.30–0.71 eV for Y_2CF_2 , indicating that Y_2CF_2 is likely to have much faster kinetics. We estimate the diffusivity D using eqn (3):⁴⁸

$$D = \frac{l^2 v_0}{2n} \exp\left(-\frac{E_{\rm A}}{kT}\right) \tag{4}$$

Here the dimensionality n=2, l is the length of a single jump, and k is the Boltzmann constant. We approximate the attempt frequency, $\nu_0=10^{13}~{\rm s}^{-1}$, a fairly typical value for fluorides; for example, the attempt frequency of BaF₂ was estimated to be $0.6\times 10^{13}~{\rm s}^{-1}$ from the frequency of the transverse optical phonon mode. ^{49,50} We obtain a negligible value of $D=2.4\times 10^{-30}~{\rm cm}^2~{\rm s}^{-1}$ for Ca₂NF at 298 K and F-poor conditions, while Y₂CF₂ has $D=1.4\times 10^{-8}~{\rm cm}^2~{\rm s}^{-1}$.

We have also used ab initio molecular dynamics (AIMD) simulations as an alternate method to calculate the intrinsic activation energy and diffusivity of stoichiometric Y2CF2 without artificially imposed defects. We run the calculations at elevated temperatures to obtain a meaningful number of diffusion events in a computationally affordable timescale. By running for 35 ps at 1700 K, 1800 K, 1900 K, 2000 K, and 2100 K, we obtain the mean-squared displacement (MSD) over time, and the diffusivity, at each temperature. Fitting the temperature-dependent diffusivities to an Arrhenius relationship provides the total activation energy.^{51,52} We find that the total activation energy of F⁻ diffusion in Y_2CF_2 is 0.75 eV \pm 0.25, which yields a diffusivity at 300 K of 6.9×10^{-16} cm² s⁻¹. These values agree well with the NEB-calculated values for the fluoride-rich condition, where F vacancies have higher formation energy and are present only at lower concentrations. In the AIMD simulations, we observe both the vacancy and interstitialcy diffusion mechanisms. However, the AIMD supercells are stoichiometric, so the defects must be generated as interstitial/vacancy pairs. For this reason, many of the hopping

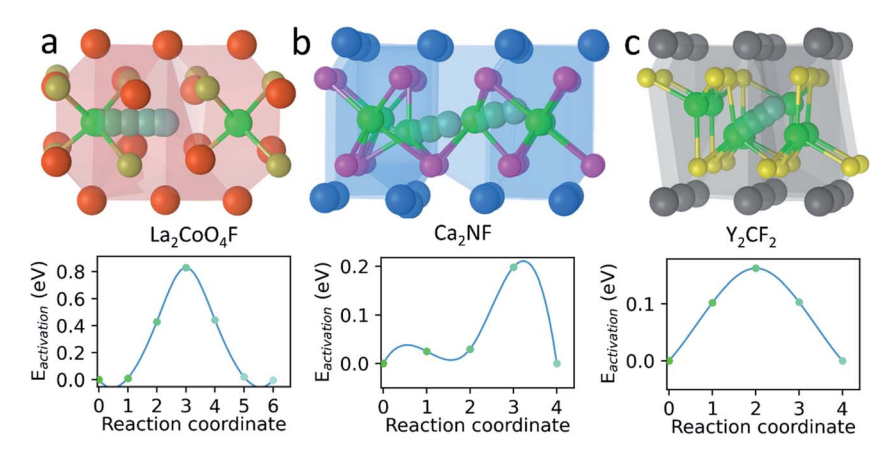


Fig. 2 NEB study of F^- diffusion kinetics. (a) Vacancy diffusion in La₂CoO₄F. A tetrahedral F^- moves to an adjacent vacant tetrahedral site in the LaO layer. The plot shows the diffusion barrier for the motion of F^- . (b) Interstitialcy mechanism in Ca₂NF. A tetrahedral F^- interstitial displaces an octahedral F^- , which moves to a tetrahedral interstitial site on the opposite side as the original. (c) Vacancy diffusion mechanism in Y₂CF₂. A tetrahedral F^- moves to an adjacent tetrahedral site.

events we observe either create or annihilate defects, as opposed to the defect-conserving mechanisms we calculate with NEB.

Experimentally, sample characteristics such as grain size will also influence the experimental diffusivity.⁵³ Since the majority of the total activation energy is the vacancy formation cost, doping Y₂CF₂ with a small amount of Ca²⁺ ought to improve the diffusion kinetics by introducing additional F- vacancies to compensate charge. Likewise, Ca2NF's interstitialcy diffusion has a low kinetic barrier height <0.2 eV, so we expect the diffusion can be enhanced by doping with Y3+ to increase Finterstitial concentration.

While Ca2N and Y2C are the most promising electrides for use in FIBs identified in this study, we have also calculated the F intercalation properties of several other electrides, including LaSi, SrSi, Ba₃N, and Ba₂NaO, ⁵⁴⁻⁵⁶ for comparison. In addition, we have calculated the stability and capacity of several known MXenes,29 which are structurally related to the layered electrides, although their chemical properties are different. We compare the theoretical performance of these different structural families in Fig. 3, with popular Li-ion electrodes shown as a reference. Ca2N and Y2C have calculated performances closest to that of their structural analogue LiCoO2, with excellent thermodynamic stability and current capacity. The other electrides are not as promising, since their structures do not allow fluoride intercalation with the same stability as the layered electrides. However, the structure alone is not enough without

the electride chemistry. The isostructural MXenes have high gravimetric capacity – up to 497 mA h g⁻¹ for Ti₂C – due to their light weight, but also have low voltage and experience large volume changes. The electride chemistry turns out to be essential because the anionic electrons have a very low work function ~2.5 eV,57 the same as Li metal.58 Because electrides give up electrons easily, they have a higher voltage vs. the cathode. The anionic electrons also improve the cycling stability by acting in combination with the large Ca²⁺ and Y³⁺ cations to maintain large interstices even in the unfluoridated state.

Our calculations suggest that Ca₂N and Y₂C can perform very well as FiB anodes. Going forward, there are several other FiB components which require improvement for these anodes to be used at their full capability. The most important target for further research is the voltage stability window of the electrolyte and the conductive additive. Ca2N is likely to form a solidelectrolyte interphase (SEI) in contact with solid fluoride electrolytes such as $La_{1-x}Ba_xF_{3-x}$ (LBF), since Li/LiF has the same potential of -2.86 V and is known to reduce LBF, ⁵⁹ while Y_2 C is right on the edge of the stability window. The effect of this SEI is not yet known, and it might be preferable to find an electrolyte which is stable against Ca2N. At the other end of the voltage window, La₂CoO₄ is the highest-voltage practical cathode, at 2.86 V vs. Ca₂N/Ca₂NF. Higher-voltage cathodes are known, such as MgFeSb₄O₄ (3.37 V)³⁰ or FeSb₂O₄ (3.49 V)³¹ but at those voltages the commonly used conductive additive, carbon black,

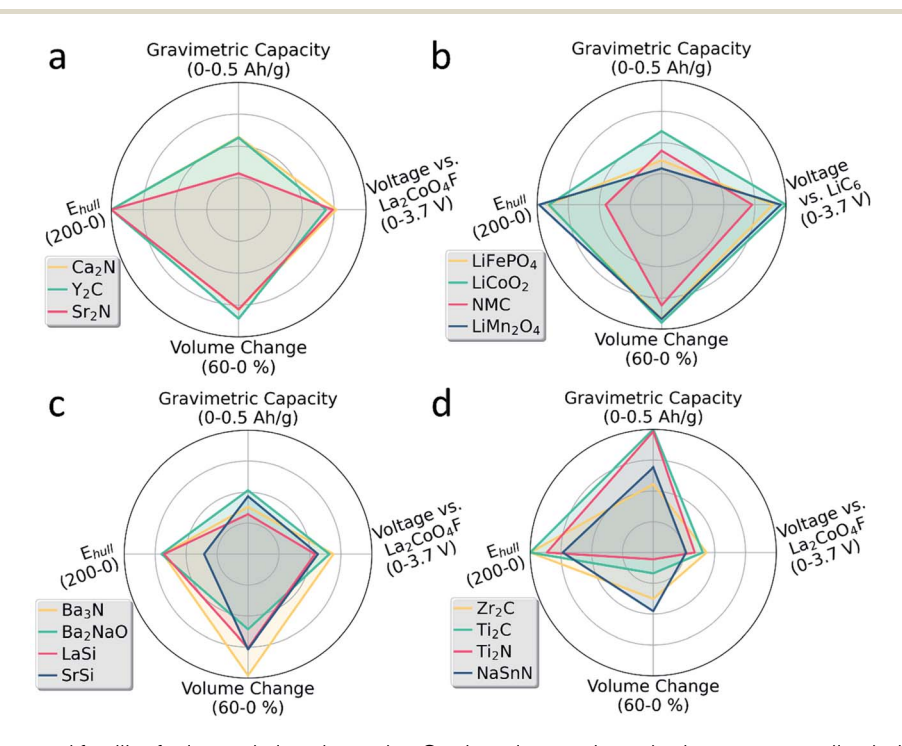


Fig. 3 Comparison of structural families for intercalation electrodes. Gravimetric capacity and voltage are normalized with respect to the highest score in each category. The voltage is the average voltage for the complete reaction with La_2CoO_4F or LiC_6 , not accounting for any steps in the voltage profile. Thermodynamic stability is measured with the hull energy E_{hull} in meV per atom, of whichever electrode state (charged or discharged) is less stable, and plotted from 200 meV above the hull to 0. Likewise, the magnitude of the volume change of the intercalated phase with respect to the de-intercalated phase is plotted from 60% to 0%. Calculated data for these and other electrodes are in ESI.† (a) The layered electrides which are the focus of this work. (b) Commercially successful Li-ion battery cathodes, for comparison. (c) Other predicted electrides with different structures than Ca₂N. (d) 2D MXenes, and the closely related material NaSnN.

reacts irreversibly with $F^{-1.3,30,59}$ The carbon fluoridation may be avoided in the future through the introduction of improved conductors such as SnO_2 or carbon nanotubes;²⁰ success in this endeavor would increase the operating voltage up to 20% if $FeSb_2O_4$ can be used, and this material is also likely to have excellent kinetics even at low temperature. In order to compete with Li-ion batteries, the accessible voltage range must be expanded to >3 V, and intercalation cathodes with higher capacities than La_2CoO_4 or $LaSrMnO_4$ are required.

In summary, we have calculated the properties of different FiB intercalation electrodes, and find that Ca_2N and Y_2C can offer an excellent combination of energy density, power density, and cycling stability. Their useful properties are due to the unique chemistry of layered electrides, which have free anionic electrons occupying vacant anion sites in the defluoridated state. Both materials intercalate F^- with very low kinetic barriers for F^- diffusion, and less volume change than most conversion electrodes, which is ideal for fast and reversible charge/discharge cycles. We expect that these new anodes will significantly advance FiBs' energy storage capability.

Authors' note

During final revision of this manuscript, a new theoretically calculated Ca₂NF phase was added to the Materials Project database. This phase has symmetry Cm; while the cation sublattice is the same as the $R\bar{3}m$ phase we identify in this work, the nitride and fluoride anions in the octahedral sites are ordered in a non-layered fashion. The Cm phase is calculated to be 26 meV per atom more stable than $R\bar{3}m$, so future work may need to consider if the nitride anions are mobile enough to re-order at battery operating temperatures.

Computational methods

We performed all DFT calculations using the VASP software, 60,61 and chose our calculation parameters to be compatible with the Materials Project database. 24,62 Certain calculations could not be converged using the tetrahedron method for electronic smearing, so these were completed using Gaussian smearing with a small SIGMA of 0.01, to minimize the discrepancy compared to the tetrahedron method. To maintain compatibility with the Materials Project, we did not include van der Waals corrections (see ESI for tests of the effects of vdW corrections†). All gravimetric capacities were calculated with respect to the mass of the defluoridated or delithiated state, and the reported voltage is the electromotive force driving the complete reaction, which does not include the "steps" seen in many experimental discharge curves due to intermediate phases. The initial locations of fluoride atoms were selected manually, a procedure which is unambiguous for the layered electrides with their clearly defined octahedral and tetrahedral sites.

We used $3 \times 3 \times 1$ supercells for the NEB calculations of Ca₂NF and Y₂CF₂, which contained 81 atoms plus the added fluorine. Ionic positions were relaxed to a force convergence criterion of 0.02 eV Å⁻¹, with two exceptions. The Y₂CF₂ interstitial diffusion was terminated after 200 steps because the F⁻

could not fit through the saddle point, and was taking an alternate route with very high energy. The saddle-point image of Ca_2NF 's interstitialcy mechanism was well-converged, but the first image could not be converged even after several hundred ionic steps. The fluorine-poor limit is defined by the Ca_2N/Ca_2NF or Y_2C/Y_2CF_2 equilibrium, while the fluorine-rich limit is the $Ca_2NF/(2CaF_2 + 0.5N_2)$ or $Y_2CF_2/(2YF_3 + C)$ equilibrium.

For the AIMD calculations, we used a slightly larger 120-atom supercell of pristine Y_2CF_2 with no defects, and used only the K-point at gamma to keep the calculations affordable. We used a plane-wave cutoff of 400 eV, a timestep of 2 fs, and kept the cell size and shape fixed. We first heated the cell from 100 K to the desired temperature over 2 ps, then allowed 5 ps for the system to reach thermal equilibrium before we began collecting diffusion data. We then calculated the diffusivity as:

$$D = \lim_{t \to \infty} \left[\frac{1}{2dt} \left\langle \left[\vec{r}(t) \right]^2 \right\rangle \right]$$
 (5)

where d=2 is the dimension of the diffusion lattice, t is the simulation time, and $\langle [r(t)]^2 \rangle$ is the time-averaged mean square displacement (MSD) of the F⁻ ions.⁶³ We obtained the activation energy by fitting the temperature-dependent diffusivity data points to an Arrhenius model:

$$D = D_0 \exp\left(-\frac{E_a}{kT}\right) \tag{6}$$

where D_0 is a constant pre-factor, E_a is the activation energy, k is Boltzmann's constant, and T is the temperature. All AIMD analysis was done using the Mo group AIMD post-processing script.⁵¹ Plots of the data are shown in ESI S4.†

Conflicts of interest

The authors declare no competing financial interest.

Acknowledgements

This work was supported by the National Science Foundation (NSF) grant numbers DMREF-1729787 and DMR-1806147. This work used computational resources of the Extreme Science and Engineering Discovery Environment (XSEDE), which is supported by NSF grant number ACI-1548562.

References

- 1 C. Helbig, A. M. Bradshaw, L. Wietschel, A. Thorenz and A. Tuma, *J. Clean. Prod.*, 2018, 172, 274–286.
- 2 D. H. Doughty and E. P. Roth, *Electrochem. Soc. Interface*, 2012, 21, 37-44.
- 3 N. Yabuuchi, K. Kubota, M. Dahbi and S. Komaba, *Chem. Rev.*, 2014, **114**, 11636–11682.
- 4 J. C. Pramudita, D. Sehrawat, D. Goonetilleke and N. Sharma, *Adv. Energy Mater.*, 2017, 7, 1602911.
- 5 J. Song, E. Sahadeo, M. Noked and S. B. Lee, *J. Phys. Chem. Lett.*, 2016, 7, 1736–1749.
- 6 D. Kundu, B. D. Adams, V. Duffort, S. H. Vajargah and L. F. Nazar, *Nat. Energy*, 2016, 1, 16119.

- 7 N. Jayaprakash, S. K. Das and L. A. Archer, Chem. Commun., 2011, 47, 12610-12612.
- 8 X. Zhao, S. Ren, M. Bruns and M. Fichtner, J. Power Sources, 2014, 245, 706-711.
- 9 X. Zhao, Z. Zhao-Karger, M. Fichtner and X. Shen, Angew. Chem., Int. Ed., 2019, 5902-5949.
- 10 M. Oka, H. Kamisaka, T. Fukumura and T. Hasegawa, Comput. Mater. Sci., 2019, 167, 92-99.
- 11 I. Mohammad, R. Witter, M. Fichtner and M. Anji Reddy, ACS Appl. Energy Mater., 2018, 1(9), 4766-4775.
- 12 V. K. Davis, C. M. Bates, K. Omichi, B. M. Savoie, N. Momčilović, Q. Xu, W. J. Wolf, M. A. Webb, K. J. Billings, N. H. Chou, S. Alayoglu, R. K. McKenney, I. M. Darolles, N. G. Nair, A. Hightower, D. Rosenberg, M. Ahmed, C. J. Brooks, T. F. Miller, R. H. Grubbs and S. C. Jones, Science, 2018, 362, 1144.
- 13 M. A. Nowroozi, K. Wissel, J. Rohrer, A. R. Munnangi and O. Clemens, Chem. Mater., 2017, 29, 3441-3453.
- 14 F. Gschwind, G. Rodriguez-Garcia, D. J. S. Sandbeck, A. Gross, M. Weil, M. Fichtner and N. Hörmann, J. Fluorine Chem., 2016, 182, 76-90.
- 15 F. Gschwind and J. Bastien, J. Mater. Chem. A, 2015, 3, 5628-5634.
- 16 C. Rongeat, M. Anji Reddy, R. Witter and M. Fichtner, ACS Appl. Mater. Interfaces, 2014, 6, 2103-2110.
- 17 M. Anji Reddy and M. Fichtner, J. Mater. Chem., 2011, 21, 17059-17062.
- 18 M. A. Nowroozi and O. Clemens, ACS Appl. Energy Mater., 2018, 1(11), 6626-6637.
- 19 D. T. Thieu, M. H. Fawey, H. Bhatia, T. Diemant, V. S. K. Chakravadhanula, R. J. Behm, C. Kübel and M. Fichtner, Adv. Funct. Mater., 2017, 27, 1701051.
- 20 L. Zhang, M. A. Reddy and M. Fichtner, J. Solid State Electrochem., 2018, 22, 997-1006.
- 21 A. Kraytsberg and Y. Ein-Eli, J. Solid State Electrochem., 2017, 21, 1907-1923.
- 22 M. A. Nowroozi, S. Ivlev, J. Rohrer and O. Clemens, J. Mater. Chem. A, 2018, 6, 4658-4669.
- 23 K. Lee, S. W. Kim, Y. Toda, S. Matsuishi and H. Hosono, Nature, 2013, 494, 336-340.
- 24 A. Jain, S. P. Ong, G. Hautier, W. Chen, W. D. Richards, S. Dacek, S. Cholia, D. Gunter, D. Skinner, G. Ceder and K. A. Persson, APL Mater., 2013, 1, 011002.
- 25 A. K. Padhi, K. S. Nanjundaswamy and J. B. Goodenough, J. Electrochem. Soc., 1997, 144, 1188-1194.
- 26 K. Mizushima, P. C. Jones, P. J. Wiseman and J. B. Goodenough, Mater. Res. Bull., 1980, 15, 783-789.
- 27 R. Shannon, Acta Crystallogr., Sect. A: Cryst. Phys., Diffr., Theor. Gen. Crystallogr., 1976, 32, 751-767.
- 28 S. V. Krivovichev, O. Mentré, O. I. Siidra, M. Colmont and S. K. Filatov, Chem. Rev., 2013, 113, 6459-6535.
- 29 M. Naguib, V. N. Mochalin, M. W. Barsoum and Y. Gogotsi, Adv. Mater., 2014, 26, 992-1005.
- 30 M. A. Nowroozi, B. de Laune and O. Clemens, ChemistryOpen, 2018, 7, 617-623.
- 31 W. Zaheer, J. L. Andrews, A. Parija, F. P. Hyler, C. Jaye, C. Weiland, Y.-S. Yu, D. A. Shapiro, D. A. Fischer, J. Guo,

- J. M. Velázquez and S. Banerjee, ACS Energy Lett., 2020, 5, 2520-2526.
- 32 K. Wissel, S. Dasgupta, A. Benes, R. Schoch, M. Bauer, R. Witte, A. D. Fortes, E. Erdem, J. Rohrer and O. Clemens, J. Mater. Chem. A, 2018, 6, 22013-22026.
- 33 A. Simon, Coord. Chem. Rev., 1997, 163, 253-270.
- 34 K. Omichi, Q. Xu and C. Brooks, US Pat. 20190103607A1, 2019.
- 35 C. Hadenfeldt and H. Herdejürgen, Z. Anorg. Allg. Chem., 1987, 545, 177-183.
- 36 A. Bowman, P. V. Mason and D. H. Gregory, Chem. Commun., 2001, 1650-1651, DOI: 10.1039/B105448C.
- 37 R. A. Nicklow, T. R. Wagner and C. C. Raymond, J. Solid State Chem., 2001, 160, 134-138.
- 38 K. Wissel, J. Heldt, P. B. Groszewicz, S. Dasgupta, H. Breitzke, M. Donzelli, A. I. Waidha, A. D. Fortes, J. Rohrer, P. R. Slater, G. Buntkowsky and O. Clemens, Inorg. Chem., 2018, 57(11), 6549-6560.
- 39 O. Clemens and R. Slater Peter, Rev. Inorg. Chem., 2013, 33, 105.
- Holland, N. Charles, J. M. Rondinelli and 40 M. K. R. Poeppelmeier, J. Am. Chem. Soc., 2016, 138, 11882-11889.
- 41 E. T. Keve and A. C. Skapski, Chem. Commun., 1966, 829-830, DOI: 10.1039/C19660000829.
- 42 W. Sun, S. T. Dacek, S. P. Ong, G. Hautier, A. Jain, W. D. Richards, A. C. Gamst, K. A. Persson and G. Ceder, Sci. Adv., 2016, 2(11), e1600225.
- 43 M. Atoji and M. Kikuchi, J. Chem. Phys., 1969, 51, 3863-3872.
- 44 D. L. Druffel, M. G. Lanetti, J. D. Sundberg, J. T. Pawlik, M. S. Stark, C. L. Donley, L. M. McRae, K. M. Scott and S. C. Warren, Chem. Mater., 2019, 31(23), 9788-9796.
- 45 A. Urban, D.-H. Seo and G. Ceder, npj Comput. Mater., 2016, 2, 16002.
- 46 K. Momma and F. Izumi, J. Appl. Crystallogr., 2011, 44, 1272-
- 47 G. Henkelman, B. P. Uberuaga and H. Jónsson, J. Chem. Phys., 2000, 113, 9901-9904.
- 48 M. Okubo, Y. Tanaka, H. Zhou, T. Kudo and I. Honma, J. Phys. Chem., 2009, 113, 2840-2847.
- 49 K.-T. Vassiliki and S. Efthimios, Open Phys., 2010, 8, 900-904.
- 50 K. Schmalzl, Phys. Rev. B, 2007, 75, 014306.
- 51 X. He, Y. Zhu, A. Epstein and Y. Mo, npj Comput. Mater., 2018, 4, 18.
- 52 X. He, Y. Zhu and Y. Mo, Nat. Commun., 2017, 8, 15893.
- 53 L. N. Patro and K. Hariharan, Solid State Ionics, 2013, 239, 41-49.
- 54 Q. Zhu, T. Frolov and K. Choudhary, *Matter*, 2019, 1(5), 1293– 1303.
- 55 L. A. Burton, F. Ricci, W. Chen, G.-M. Rignanese and G. Hautier, Chem. Mater., 2018, 30, 7521-7526.
- 56 T. Tada, S. Takemoto, S. Matsuishi and H. Hosono, Inorg. Chem., 2014, 53, 10347-10358.
- 57 M. M. Menamparambath, J.-H. Park, H.-S. Yoo, S. P. Patole, J.-B. Yoo, S. W. Kim and S. Baik, Nanoscale, 2014, 6, 8844-8851.
- 58 P. A. Anderson, Phys. Rev., 1949, 75, 1205-1207.

- 59 A. Grenier, A. G. Porras-Gutierrez, M. Body, C. Legein, F. Chrétien, E. Raymundo-Piñero, M. Dollé, H. Groult and D. Dambournet, J. Phys. Chem. C, 2017, 121, 24962-24970.
- 60 G. Kresse and D. Joubert, Phys. Rev. B, 1999, 59, 1758-1775.
- 61 G. Kresse and J. Furthmüller, Phys. Rev. B, 1996, 54, 11169-11186.
- 62 S. P. Ong, W. D. Richards, A. Jain, G. Hautier, M. Kocher, S. Cholia, D. Gunter, V. L. Chevrier, K. A. Persson and G. Ceder, Comput. Mater. Sci., 2013, 68, 314-319.
- 63 Y. Mo, S. P. Ong and G. Ceder, Chem. Mater., 2012, 24, 15-17.